Chin A Yi, MD
Kyung Soo Lee, MD
Eun A Kim, MD
Joungho Han, MD
Hojoong Kim, MD
O Jung Kwon, MD
Yeon Joo Jeong, MD
Seonwoo Kim, PhD

Index terms:
Lung neoplasms, 68.3115, 68.3221
Lung neoplasms, CT, 68.12113, 68.12114, 68.12115
Lung neoplasms, diagnosis

Published online before print
10.1148/radiol.2331031535
Radiology 2004; 233:191–199

Abbreviation:
VEGF = vascular endothelial growth factor

[1] From the Department of Radiology and Center for Imaging Science (C.A.Y., K.S.L., Y.J.J.), Department of Pathology (J.H.), Department of Internal Medicine, Division of Pulmonary and Critical Care Medicine (H.K., O.J.K.), and Biostatistics Unit, Samsung Biomedical Research Institute (S.K.), Samsung Medical Center, Sungkyunkwan University School of Medicine, 50 Ilwon-Dong, Kangnam-Ku, Seoul 135–710, Korea; and Department of Radiology, National Cancer Center Hospital, Koyang, Korea (E.A.K.). Received September 29, 2003; revision requested December 10; revision received December 30; accepted January 30, 2004. Supported in part by a research grant from the Korean Organization of Science and Engineering Foundation (grant no. R01–2001-00109). **Address correspondence to** K.S.L. (e-mail: *melon2@samsung.co.kr*).

Authors stated no financial relationship to disclose.

Author contributions:
Guarantor of integrity of entire study, K.S.L.; study concepts and design, C.A.Y., K.S.L., E.A.K.; literature research, C.A.Y., E.A.K.; clinical studies, H.K., O.J.K.; data acquisition, C.A.Y., K.S.L., E.A.K., J.H., H.K., O.J.K., Y.J.J.; data analysis/interpretation, C.A.Y., K.S.L., E.A.K., Y.J.J.; statistical analysis, C.A.Y., K.S.L., S.K.; manuscript preparation and definition of intellectual content, C.A.Y., K.S.L.; manuscript editing, revision/review, and final version approval, all authors

Solitary Pulmonary Nodules: Dynamic Enhanced Multi–Detector Row CT Study and Comparison with Vascular Endothelial Growth Factor and Microvessel Density[1]

PURPOSE: To evaluate enhancement dynamics of solitary pulmonary nodules at multi–detector row computed tomography (CT) and to correlate results with extent of tumor angiogenesis in pathologic specimens.

MATERIALS AND METHODS: One hundred thirty-one patients with solitary pulmonary nodules underwent unenhanced thin-section CT, followed by dynamic helical CT (throughout the nodule for 30 mm along the *z*-axis [13 images] and at 20-second intervals for 3 minutes [130 images total]) after intravenous injection of 120 mL of contrast medium. Diagnosis of malignancy or benignancy was assigned in 109 patients, and follow-up imaging suggested benignancy in the remaining 22. CT findings were analyzed for peak attenuation, net enhancement, and enhancement dynamics. In 54 patients with surgical diagnoses, Pearson correlation coefficient was used to correlate enhancement pattern with extent of microvessel density and vascular endothelial growth factor (VEGF) staining.

RESULTS: With 30 HU or more of net enhancement as a cutoff value in differentiation of malignant and benign nodules, sensitivity for malignant nodules was 99% (69 of 70 malignant nodules), specificity was 54% (33 of 61 benign nodules), positive predictive value was 71% (69 of 97 malignant readings), negative predictive value was 97% (33 of 34 benign readings), and accuracy was 78% (102 of 131 nodules). Peak attenuation was correlated positively with extent of microvessel density ($r = 0.369$, $P = .006$) and VEGF staining ($r = 0.277$, $P = .042$). Malignant nodules showed significantly higher VEGF expression ($P = .009$) than that of benign nodules.

CONCLUSION: Dynamic enhancement with multi–detector row CT shows high sensitivity and negative predictive values for diagnosis of malignant nodules but low specificity because of highly enhancing benign nodules. Extent of enhancement reflects underlying nodule angiogenesis.

Information on the morphologic features and attenuation values of a peripheral pulmonary nodule on unenhanced thin-section computed tomographic (CT) images may be insufficient to allow the differentiation of benign and malignant nodules (1). The evaluation of tumor vascularity with contrast material–enhanced CT has proved to be useful in the differentiation of malignant and benign nodules (2–9). In previous dynamic CT studies in which a conventional or single–detector row helical CT machine was used, however, investigators acquired a single scan or a limited number of scans through the nodule at specific times (usually at 1-minute intervals, with scans obtained at 1, 2, 3, and 4 minutes after intravenous injection of contrast medium) for the duration of the dynamic study (2,3,7,9).

Therefore, a small number of CT scans obtained in a nodule at a given time may have led to partial volume effect, artifact, and difficulties in terms of reproducibility, mainly resulting from patient variations in breath holding. These limitations may have also made it difficult to compare directly the attenuation values of nodules at the same level on CT scans acquired at different times. Furthermore, because images were obtained at 1-minute intervals, changes in detailed attenuation values between each minute would have been unavailable, making it difficult to evaluate the actual peak attenuation value and the peak enhancement time.

With the advent of multi–detector row CT, we have the advantage of shorter acquisition times, greater coverage, and superior image resolution along the z-axis (10). Image clusters obtained at a given time throughout a nodule can be acquired sequentially by using a helical technique at short time intervals after the intravenous injection of contrast medium, thus allowing the same or very similar scans to be obtained through the nodule at various times to compare the extent of enhancement.

A growing malignant nodule needs its own blood supply from adjacent tissues, which is essentially required for tumor growth and metastatic spread. This process may be caused by the increased release of angiogenic factors from the malignant nodule, such as vascular endothelial growth factor (VEGF), and the subsequent increase in extent of microvessel density (11–14). The increased extent of microvessel density leads to increased perfusion and permeability of the capillaries and is associated frequently with strong enhancement of a malignant nodule at CT (15,16). Therefore, the extent of enhancement can be interpreted as reflecting tumor vascularity, which may aid in the differentiation of malignancy and benignancy.

The purpose of this study was to evaluate the enhancement dynamics of solitary pulmonary nodules by using multi–detector row CT and to correlate the results with the extent of tumor angiogenesis in pathologic specimens.

MATERIALS AND METHODS

Patients and CT Scanning

From March 2002 to March 2003, a total of 198 patients (157 men and 41 women; age range, 24–82 years; mean age, 56 years) with a solitary pulmonary nodule at chest radiography (approximately spherical; short- and long-axis diameters were within a factor of 1.5 of each other) underwent dynamic chest CT with a four–detector row CT scanner (LightSpeed QX/i; GE Medical Systems, Milwaukee, Wis). The institutional review board of Samsung Medical Center approved the study protocol for this CT study, and written informed consent was obtained from all patients.

Before dynamic CT was performed, we obtained targeted thin-section helical CT scans (2.5-mm collimation, 0.8-second gantry rotation time, 120 kVp, 70 mA) through the nodule. Nodules that appeared to be solitary at chest radiography but appeared to have satellite nodules at CT (n = 2) were included in this study. For nodules with satellite lesions, only the main nodule was evaluated with dynamic enhanced CT. If nodules contained benign calcifications (diffuse, laminated, popcorn-like, or central) at thin-section CT, they were excluded (n = 5). Nodules that contained fat at thin-section CT were also excluded (n = 1). Nodules with stippled (n = 3) or peripheral nodular (n = 2) calcifications were included. Dynamic CT was performed in the remaining 192 patients.

Before the intravenous injection of contrast medium, a series of 13 images was obtained throughout the nodule for 30 mm along the z-axis with 2.5-mm collimation[b], 120 kVp, 170 mA, 0.8-second gantry rotation time, and a table speed of 3.75 mm/sec over 8 seconds. Thereafter, an additional nine series of images were obtained at 20-second intervals for 3 minutes after contrast medium injection (3 mL/sec, total of 120 mL of iomeprol, Iomeron 300; Bracco, Milan, Italy) with a power injector (MCT Plus; Medrad, Pittsburgh, Pa) with the same parameters used for the initial preenhancement series (10 total series of images obtained at 0, 20, 40, 60, 80, 100, 120, 140, 160, and 180 seconds).

Immediately after dynamic imaging, low-dose (50 mA, 120 kVp, 5-mm collimation, table speed of 15 mm/sec) helical CT scans were obtained from the lung apices to the level of the middle pole of both kidneys for tumor staging. Image data were reconstructed with a thickness of 2.5 mm (13 images in each cluster; total number of dynamic images, 130 [13 images × 10 series]) by using a standard algorithm. All thin-section and dynamic CT data were interfaced directly to our picture archiving and communication system, or PACS (Integrated Imaging Solutions, version 8.1; GE Medical Systems, Mt Prospect, Ill), which displayed all image data on monitors (four monitors, 1536 × 2048 image matrices, 8-bit viewable gray scale, and 60-foot-lambert luminescence). On the monitors, both mediastinal (window width, 400 HU; window level, 20 HU) and lung (window width, 1500 HU; window level, −700 HU) window images were viewed.

The technical adequacy of dynamic CT fulfilled the following criteria, as presented in previous studies (7,9): absence of the extravasation of contrast medium at the site of injection, appropriate enhancement of the cardiovascular structures imaged during examination, no marked reaction to contrast medium that interfered with image acquisition, and satisfactory patient respiratory registration without artifact on equatorial images.

In two patients, inconsistent breath hold was a problem for obtaining dynamic image clusters at the same level. In another two patients, the nodules were too small (8 and 9 mm in diameter) to measure the attenuation value (partial volume averaging precluded the measurement of attenuation value). With the exception of these four patients, the dynamic images were technically adequate for 188 patients, and no serious reactions to contrast medium were reported. No examination was interrupted because of contrast medium reaction.

Of 188 patients, 57 were excluded because they had neither histopathologic diagnosis nor follow-up information. The remaining 131 patients (82 men with a mean age of 58 years and an age range of 24–82 years; 49 women with a mean age of 52 years and an age range of 25–73 years; all individuals, mean age of 56 years and age range of 24–82 years) were included. These patients underwent transthoracic needle biopsy (n = 39) or surgery (n = 70), which included lobectomy (n = 64) and wedge resection (n = 6). Twenty-two patients in whom CT findings and clinical situations suggested benignancy of a nodule but histopathologic diagnosis was not assigned were regarded to have a benign nodule because the nodules did not change in size (n = 12), showed a decrease in size (n = 2), or disappeared (n = 8). Nodules without size change were followed up with imaging for more than 12 months (mean, 13 months; range, 12–21 months).

Radiation Exposure

Radiation exposure was determined by means of thermoluminescent dosimetry, as described in the study of Jung et al (17). Total organ doses of thin-section, dynamic, and low-dose CT studies were

calculated. Four lithium fluoride chips were placed in the bilateral upper and lower lung zones of the irradiated lungs of the phantom: one in the right upper lung zone, one in the left upper lung zone, one in the right lower lung zone, and one in the left lower lung zone.

Radiation doses were measured twice: once with the presumption that the nodule was located in the upper lung zone and twice with the presumption that the nodule was located in the lower lung zone. The radiation doses (at nodule sites and at other lung sites away from the nodule locations) were calculated by measuring the absorbed doses in lithium fluoride chips placed inside the phantom. The measured organ dose was compared with that of standard thoracic helical CT (beam collimation of 20 mm, beam pitch of 0.75, 0.8-second rotation time, 120 kVp, and 210 mA) at our institution.

Evaluation of Enhancement Dynamics

After viewing all 130 images as thumbnail images on PACS monitors, we selected one image for analysis from 13 images at a given time. The selected image was the transverse section with the largest diameter (scanned at the equator of the nodule). We measured the attenuation value of the nodule in the same area on the selected image for each cluster at each time (from unenhanced image to image acquired at 3 minutes). We examined a region of interest that covered about one-half of the diameter of the nodule at the equator and excluded calcified, cystic, or necrotic areas. The edges of the nodule were avoided to prevent partial volume averaging. All measurements in Hounsfield units were obtained from mediastinal window images to ensure that partial volume averaging was minimized. All measurements were obtained at the time of CT examination without knowledge of the histologic diagnosis.

Two radiologists with 2 years (C.A.Y.) and 14 years (K.S.L.) of experience in chest CT measured the attenuation values independently. We analyzed the extent of tumor enhancement by using peak and net enhancement. Peak enhancement was defined as a maximum attenuation value of the nodule over the entire duration of the dynamic study. Net enhancement was calculated by subtracting preenhancement attenuation from peak enhancement attenuation. The maximum diameter of the nodule was also measured.

The dynamics of enhancement were assessed by using two indexes: the maximum relative enhancement ratio and the slope of enhancement. Time to peak enhancement (expressed in seconds) was also recorded. The maximum relative enhancement ratio was calculated by subtracting preenhancement attenuation from peak enhancement attenuation and then dividing the result by preenhancement attenuation. The slope of enhancement (expressed in seconds^{-1}) was determined by dividing the maximum relative enhancement ratio by the time to peak attenuation (18).

Pathologic Evaluation

One experienced lung pathologist (J.H.) with 12 years of experience in lung pathology recorded the histologic diagnosis of each nodule. For each nodule, microvessel density and VEGF expression were assessed by means of immunohistochemistry to investigate neovascularization and angiogenic activity (15).

Immunohistochemical Staining

After acquisition of slices for ordinary hematoxylin-eosin staining, the avidin-biotin complex method was used for immunostaining. Slices (4–5-μm thickness) from at least one representative block of formalin-fixed paraffin-embedded tissue in each case were deparaffinized and dehydrated in graded alcohols. Heat-induced antigen retrieval was performed by using a microwave oven and citrate buffer (pH, 6.0; 10 mol/L). All samples were immunostained by using the streptomycin avidin-biotin complex technique with monoclonal antibodies against VEGF (polyclonal, Santa Cruz Biotech, Santa Cruz, Calif; 1:80 dilution) and CD31 (Clone JC/70A, Dako, Glostrup, Denmark; 1:40 dilution), which is mainly expressed on small-vessel endothelial cells. Staining was performed by using an automatic immunostainer (TechMate; Dako) and the LSAB detection system with diaminobenzidine as the chromogen (ChemoMate; Dako). Appropriate positive and negative controls were run simultaneously.

Evaluation of Immunostaining for VEGF and Microvessel Density

Fifty-four nodules were evaluated by means of immunostaining for tumor angiogenesis. All slides were coded and evaluated by one pathologist (J.H.) with 5 years of experience in immunostaining for VEGF and microvessel density, who was unaware of the results of the dynamic CT nodule studies.

The VEGF staining was graded in terms of its extent and intensity. Extent was subdivided into four degrees according to the percentage of tumor cells that showed higher levels of staining than the background. Nodules with up to 25% of tumor cells that stained for VEGF were scored as 1, 26%–50% as 2, 51%–75% as 3, and 76%–100% as 4. Intensity was subdivided into three degrees—weak, moderate, and strong—for which scores of 1, 3, and 5 were given, respectively. Criteria for intensity of staining were as follows: weak staining, negative or faint cytoplasmic staining for VEGF; moderate staining, weak (light brown in color) or diffuse homogeneous cytoplasmic staining for VEGF (included focal strong staining but less than 10% in approximation of observed cells); and strong staining, diffuse granular dark brown cytoplasmic staining for VEGF that included at least 10% of observed cells. The total score (maximum of 9) of VEGF staining was calculated by adding the extent (maximum of 4) and intensity (maximum of 5).

The degree of angiogenesis was determined by means of microvessel density in the defined areas of tissue sections according to the method of Weidner et al (11). Each microvessel count was performed twice. Each slide was first scanned at low magnification (×100) to determine three "hot spot" areas where the number of microvessels was at a maximum. Areas of focal sclerosis or necrosis were excluded. Microvessel density was counted in each of the three hot-spot areas on slides. Areas of staining with no discrete breaks were counted as a single vessel. Microvessel density was determined by adding the number of vessels in each of the three hot spots.

Data and Statistical Analysis

The Mann-Whitney test was used to analyze statistical differences in age between groups of men and women who underwent dynamic enhanced CT and whose results were analyzed.

Diagnostic characteristics—that is, sensitivity, specificity, accuracy, positive predictive value, and negative predictive value—were calculated retrospectively at different levels of cutoff value for discrimination between malignant and benign nodules. Differences in measured attenuation values of nodules between two observers were analyzed by calculating intraclass correlation coefficients.

The student *t* test was used to analyze

TABLE 1
Diagnoses of 131 Nodules

Nodule Type and Diagnosis	No. of Nodules
Malignant	70 (53)
Adenocarcinoma	43 (61)
Squamous cell carcinoma	13 (19)
Metastatic carcinoma	6 (9)
Pheomorphic carcinoma	2 (3)
Large-cell neuroendocrine carcinoma	2 (3)
Mucoepidermoid carcinoma	2 (3)
Carcinoid tumor	1 (1)
Small-cell lung cancer	1 (1)
Benign*	61 (47)
Focal pneumonia without specific microorganism	12 (31)
Tuberculoma	9 (23)
Hamartoma	9 (23)
Sclerosing hemangioma	5 (13)
Intrapulmonary lung nodule	2 (5)
Inflammatory pseudotumor	1 (3)
Fungal granuloma	1 (3)

Note.—Numbers in parentheses are percentages.
* Twenty-two benign nodules (36%) were diagnosed by means of follow-up imaging; 39 (64%) were diagnosed by means of pathologic examination.

TABLE 2
Nodule Characteristics

Characteristic	Malignant Nodules (n = 70)	Benign Nodules (n = 61)	P Value
Peak enhancement (HU)			
Mean ± SD	98 ± 17	78 ± 30	<.001*
Median	94	74	
Range	63–160	30–132	
Net enhancement (HU)			
Mean ± SD	53 ± 15	35 ± 26	<.001†
Median	51	28	
Range	27–106	1–88	
Preenhancement value (HU)			
Mean ± SD	46 ± 9	44 ± 12	.303†
Median	46	43	
Range	10–68	13–85	
Diameter (mm)			
Mean ± SD	22 ± 6	20 ± 6	.642*
Median	21	18	
Range	9–30	8–30	
Maximum relative enhancement ratio			
Mean ± standard error	1.267 ± 0.107	0.848 ± 0.097	<.001†
95% Confidence interval	1.053, 1.482	0.654, 1.043	
Time to peak enhancement (sec)			
Mean ± SD	103 ± 43	119 ± 45	.033†
Median	100	120	
Range	40–180	40–180	
Slope of enhancement (sec^{-1})			
Mean ± standard error	0.015 ± 0.013	0.009 ± 0.006	<.001†
95% Confidence interval	0.012, 0.017	0.007, 0.011	

Note.—SD = standard deviation.
* Student t test.
† Mann-Whitney test.

the statistical significance of the extent of peak enhancement and the extent of microvessel density between malignant and benign nodules. The Mann-Whitney test was used to analyze statistical differences in attenuation value on preenhancement images, net enhancement, maximum relative enhancement ratio, time to peak enhancement, slope of enhancement, and extent of VEGF staining in malignant and benign nodules. Pearson correlation coefficients were used to represent the relationships between the extent of nodule enhancement and microvessel densities and the VEGF scores. P values less than .05 were considered to indicate a statistically significant difference.

RESULTS

The measured total organ dose with thin-section, dynamic, and low-dose CT ranged from 185.8 to 191.6 mGy at nodule sites. Organ dose ranged from 24.2 to 25.7 mGy elsewhere in the lungs. In a standard thoracic helical CT examination at our institution, organ dose ranges from 38.7 to 39.5 mGy.

In the 131 patients, men (n = 82) were significantly older than women (n = 49) (P = .008).

Extent of Enhancement according to Histologic Findings

Of 131 nodules, 70 (53%) proved to be malignant, and 61 (47%) were benign (Table 1). The sizes of 131 nodules were as follows: smaller than 10 mm in two patients, 10–20 mm in 52 patients, and larger than 20 mm in 77 patients.

Peak enhancement, preenhancement attenuation, net enhancement, diameter of all nodules, maximum relative enhancement ratio, time to peak enhancement, and slope of enhancement are summarized in Table 2. Malignant nodules (mean attenuation, 98 HU; range, 63–160 HU) (Figs 1, 2) showed significantly higher peak enhancement than that of benign nodules (mean attenuation, 78 HU; range, 30–132 HU) (P < .001) (Fig 3). Attenuation values on preenhancement images were not significantly different for malignant (mean, 46 HU; range, 10–68 HU) and benign (mean, 44 HU; range, 13–85 HU) nodules (P = .303). Therefore, the net enhancement of malignant nodules (mean, 53 HU; range, 27–106 HU) was significantly higher than that of benign nodules (mean, 35 HU; range, 1–88 HU) (P < .001). Statistical differences were observed in the enhancement dynamics of malignant and benign nodules. Malignant nodules showed significantly higher maximum relative enhancement ratio, shorter time to peak enhancement, and steeper slope of enhancement. Good interobserver agreement was obtained between two observers in terms of measuring the attenuation values of nodules (intraclass correlation coefficient, 0.8789–0.9751; P < .001).

When less than 30 HU of net enhancement is used as a cutoff value at CT, sensitivity in the diagnosis of malignant nodules was 100%, but specificity was low—less than 50%. When more than 30 HU of net enhancement is used as a cutoff value, sensitivity in the diagnosis of malignant nodules decreased, which raised the possibility of false-negative diagnosis of truly malignant nodules (Table 3). When 30 HU of net enhancement is used as a cutoff value, 97 nodules were considered malignant with higher enhancement than the cutoff value, whereas 34 nodules were considered benign.

By using the same cutoff value, sensitivity for malignant nodules was 99% (69 of 70 malignant nodules), specificity was 54% (33 of 61 benign nodules), positive predictive value was 71% (69 of 97 malignant readings), negative predictive value was 97% (33 of 34 benign readings), and

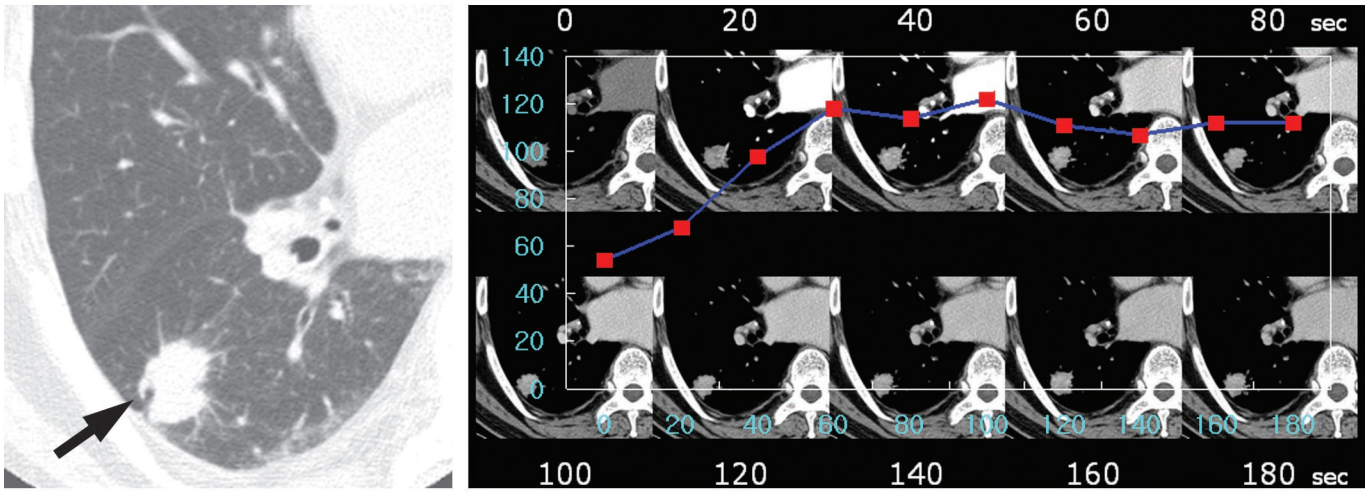

a. b.

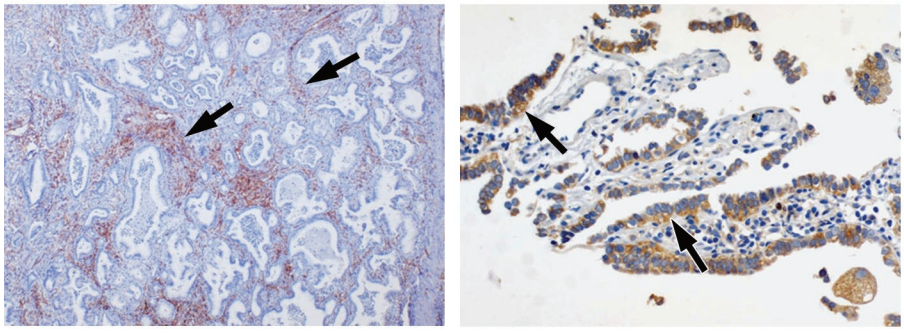

c. d.

Figure 1. Adenocarcinoma in a 76-year-old man. **(a)** Lung window of transverse thin-section (2.5-mm collimation) CT scan obtained at level of right basal trunk shows 22-mm nodule (arrow) with lobulated and spiculated margin in right lower lobe. **(b)** Serial images obtained at 20-second intervals and at similar levels show enhancement dynamics of nodule. Peak enhancement is 122 HU; net enhancement, 68 HU; maximum enhancement ratio, 1.259; slope of enhancement, 0.013; and time to peak enhancement, 100 seconds. **(c)** Microvessel density with CD31 immunostaining is 87. Vessel wall (arrows) is stained dark brown. (Original magnification, ×40.) **(d)** VEGF is 7. Intracytoplasmic brown pigments (arrows) indicate VEGF. (Original magnification, ×100.)

accuracy was 78% (102 of 131 nodules) (Tables 3, 4). A false-negative case was seen in a patient with adenocarcinoma of the lung, which showed 27 HU of net enhancement. False-positive results were obtained for six of nine (67%) tuberculomas (Fig 4), four of four (100%) sclerosing hemangiomas, two of nine (22%) hamartomas, one (100%) blastomycoma, one (100%) inflammatory pseudotumor, one (100%) intrapulmonary lymph node, and three of 12 (25%) other unspecified nodules.

Correlation of Enhancement and Histopathologic Findings

The extent of tumor angiogenesis in malignant and benign nodules is summarized in Table 5. VEGF expression was significantly different in malignant and benign nodules ($P = .009$). No significant difference was noted in the extent of microvessel density between malignant and benign nodules. Significant positive correlations were found between the extent of peak enhancement and microvessel density ($r = 0.369$, $P = .006$) and between peak enhancement and VEGF ($r = 0.277$, $P = .042$) (Table 6). The extent of net enhancement was not found to be correlated significantly with microvessel density or VEGF.

DISCUSSION

In previous studies on the usefulness of contrast-enhanced CT for the differentiation of malignant and benign nodules, the mean peak enhancement of malignant nodules was approximately 40 HU (range, 41.9–46.5 HU) (4,7–9). In the present study, however, the mean peak enhancement of malignant nodules was much higher, reaching 98 HU. This discrepancy may be explained as follows. First, in previous studies (2,3,7,9), the injection rate and total amount of contrast material were 2 mL/sec and 100 mL, respectively. In the current study, however, they were 3 mL/sec and 120 mL, respectively. This may have led to more enhancement than in previous studies. Second, in our study, we used a shorter acquisition time interval (20 seconds) than that in previous studies (usually 1-minute intervals). This shorter interval enabled us to obtain a more detailed time-attenuation curve by identifying the detailed changes in attenuation values of nodules for the entire duration of dynamic imaging.

Third, 13 images were acquired at a given time in the present study, which is more than in previous studies (mostly one but up to 10 images). By obtaining more images at a given time, our methods might have facilitated selection of exactly the same level of images through-

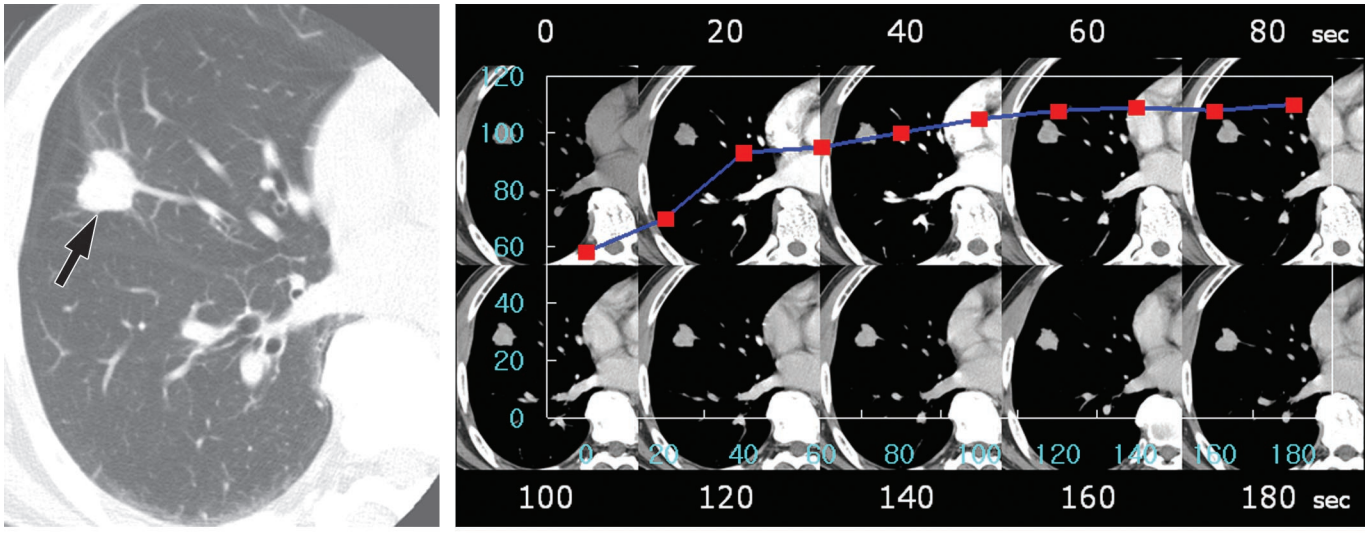

a. b.

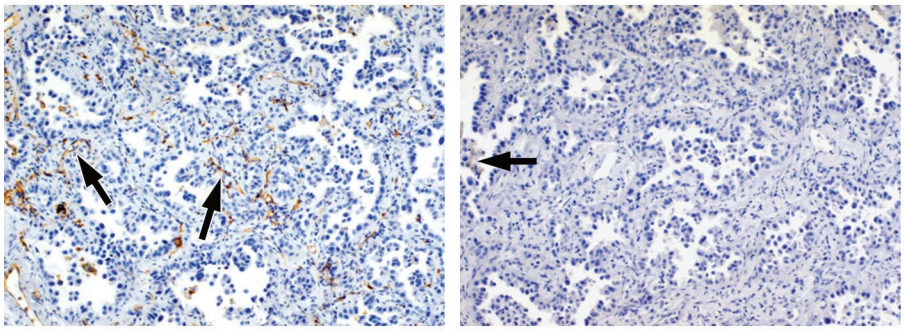

c. d.

Figure 2. Adenocarcinoma in a 64-year-old man. **(a)** Lung window of transverse thin-section (2.5-mm collimation) CT scan obtained at level of right inferior pulmonary vein shows 21-mm nodule (arrow) with lobulated and spiculated margin in right middle lobe. **(b)** Serial images obtained at 20-second intervals and at similar levels show enhancement dynamics of nodule. Peak enhancement is 110 HU; net enhancement, 52 HU; maximum enhancement ratio, 0.906; slope of enhancement, 0.005; and time to peak enhancement, 180 seconds. **(c)** Microvessel density with CD31 immunostaining is 67. Vessel wall (arrows) is stained dark brown. (Original magnification, ×40.) **(d)** VEGF is 3. Intracytoplasmic brown pigments (arrow) indicate VEGF. (Original magnification, ×40.)

TABLE 3
Diagnostic Rates of Dynamic Enhancement CT according to Various Thresholds of Cutoff Values

Parameter	15-HU Threshold	20-HU Threshold	25-HU Threshold	30-HU Threshold	35-HU Threshold	40-HU Threshold
Sensitivity (%)	100	100	100	99	93	84
Specificity (%)	36	41	44	54	54	54
Accuracy (%)	70	73	74	78	75	70
Positive predictive value (%)	64	67	67	71	70	68
Negative predictive value (%)	100	100	100	97	87	75

out the nodule for comparison. Therefore, the attenuation values of nodules were more complete than those in previous studies, in which only a limited number of scans were obtained through the nodule at a given time. Fourth, respiratory misregistration was reduced in our study. Inadequate images caused by inconsistent breath hold after injection of contrast medium were obtained in only two of 192 (1%) patients. In previous studies, the rates of technically inadequate studies ranged from 3% (19 of 550 patients) to 10% (21 of 218 patients) (3,9).

Yamashita et al (4) reported that a maximum attenuation of 20–60 HU appears to be a good predictor of malignancy. Also noteworthy is a report by Swensen et al (9) in 2000, in which a threshold value of 15 HU produced a sensitivity of 98%, a specificity of 58%, and an accuracy of 77% for malignant nodules. Since then, the cutoff values for differentiation of benign and malignant nodules have been set at 15 or 20 HU. In our dynamic study in which multi–detector row CT was used, however, higher peak enhancement was obtained, and thus higher attenuation values could be used as cutoff values for this differentiation.

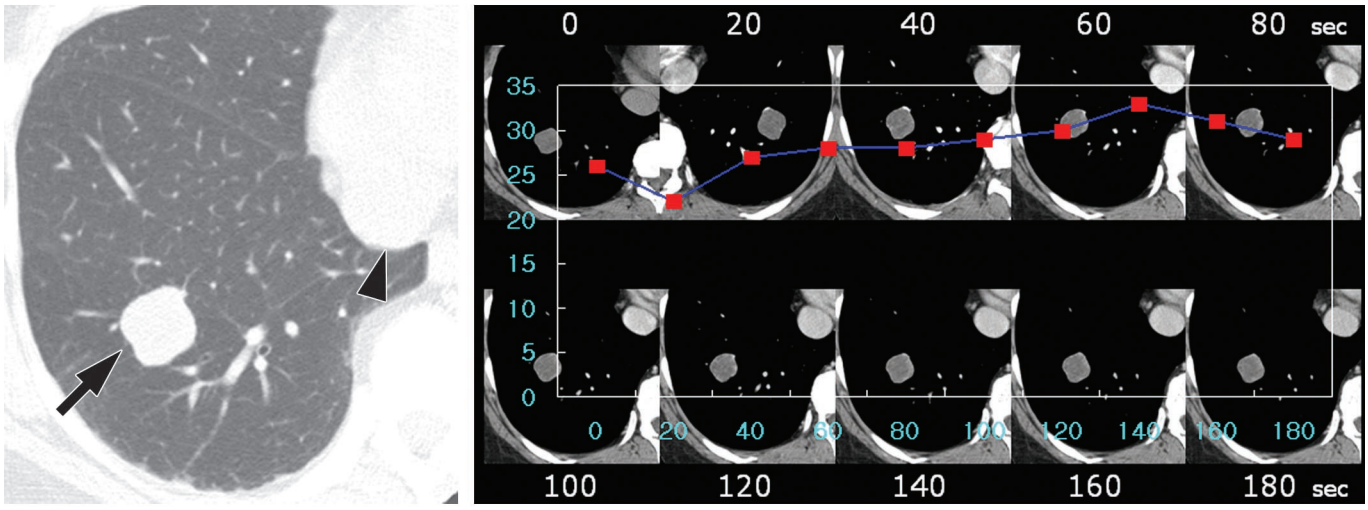

a. b.

Figure 3. Hamartoma in a 50-year-old woman. **(a)** Lung window of transverse thin-section (2.5-mm collimation) CT scan obtained at level of suprahepatic inferior vena cava (arrowhead) shows 20-mm nodule (arrow) with slightly lobulated margin in right lower lobe. **(b)** Serial images obtained at 20-second intervals and at similar levels show enhancement dynamics of nodule. Peak enhancement is 33 HU; net enhancement, 7 HU; maximum enhancement ratio, 0.267; slope of enhancement, 0.002; and time to peak enhancement, 140 seconds. Microvessel density with CD31 immunostaining was 15, and VEGF was 2 (not shown).

TABLE 4
Enhancement of 131 Nodules according to Diagnosis

Enhancement	No. of Malignant Nodules (n = 70)	No. of Benign Nodules (n = 61)
≥30 HU (n = 97)	69	28
<30 HU (n = 34)	1	33

TABLE 5
Extent of Tumor Angiogenesis in 54 Malignant and Benign Nodules

Parameter and Nodule Type	Mean Value ± Standard Deviation
Microvessel density*	
Malignant (n = 39)	51.2 ± 24.2
Benign (n = 15)	38.2 ± 25.6
VEGF†	
Malignant (n = 38)	6.8 ± 2.3
Benign (n = 16)	4.8 ± 2.6

* P = .572 with the Student t test.
† P = .009 with the Mann-Whitney test.

Actually, with a cutoff value of 30 HU of net enhancement, overall diagnostic accuracy in terms of differentiation of benign and malignant nodules—that is, sensitivity for malignant nodules of 99%, specificity of 54%, positive predictive value of 71%, negative predictive value of 97%, and accuracy of 78%, is similar to that in previous studies. We could have increased the negative predictive value by maintaining high sensitivity with higher cutoff values than those in previous studies. Except for active granulomas and vascular tumors such as sclerosing hemangiomas, most benign nodules showed enhancement values of less than 30 HU. Therefore, when a nodule shows enhancement of less than 30 HU, a benign nodule can be diagnosed with confidence.

In terms of analysis of enhancement dynamics, malignant nodules showed characteristic enhancement patterns and dynamics, not only with respect to significantly higher peak and net enhancements but also with respect to shorter time to peak enhancement and steeper slope of enhancement. This could be explained by the higher microvessel density (mean, 51) of malignant nodules versus that of benign nodules (mean, 38), but these values were not significantly different (P = .572).

Not only was the extent of VEGF expression greater in malignant nodules, but microvessel density was higher; however, only VEGF expression was significantly higher in malignant nodules (P = .009). This insignificantly higher level of microvessel density expression in malignant nodules may be explained as follows. First, we analyzed the enhancement patterns and dynamics in 131 patients with a solitary pulmonary nodule, but only 53 patients were included in the analysis for tumor angiogenesis. Therefore, true-negative cases (benign nodules), which showed little enhancement and which were later found to be benign by means of percutaneous needle aspiration biopsy, were excluded from the tumor angiogenesis analysis. These benign nodules were excluded because tumor angiogenesis could not be assessed by means of an aspiration biopsy specimen alone. Moreover, many highly enhancing benign nodules, such as active granulomas or sclerosing hemangiomas, were removed surgically because of the risk of malignancy and were included selectively in immunostaining for tumor angiogenesis.

Significant positive correlations were found between the extent of peak enhancement and tumor angiogenesis of microvessel density (r = 0.369, P = .006) or VEGF (r = 0.277, P = .042), irrespective of the malignant or benign nature of the nodules. Yamashita et al (5) suggested that the number of small vessels (microvessels) (0.02–0.10-mm inner diameter) might reflect the extent of enhancement of lung carcinoma at incremental CT more than the number of

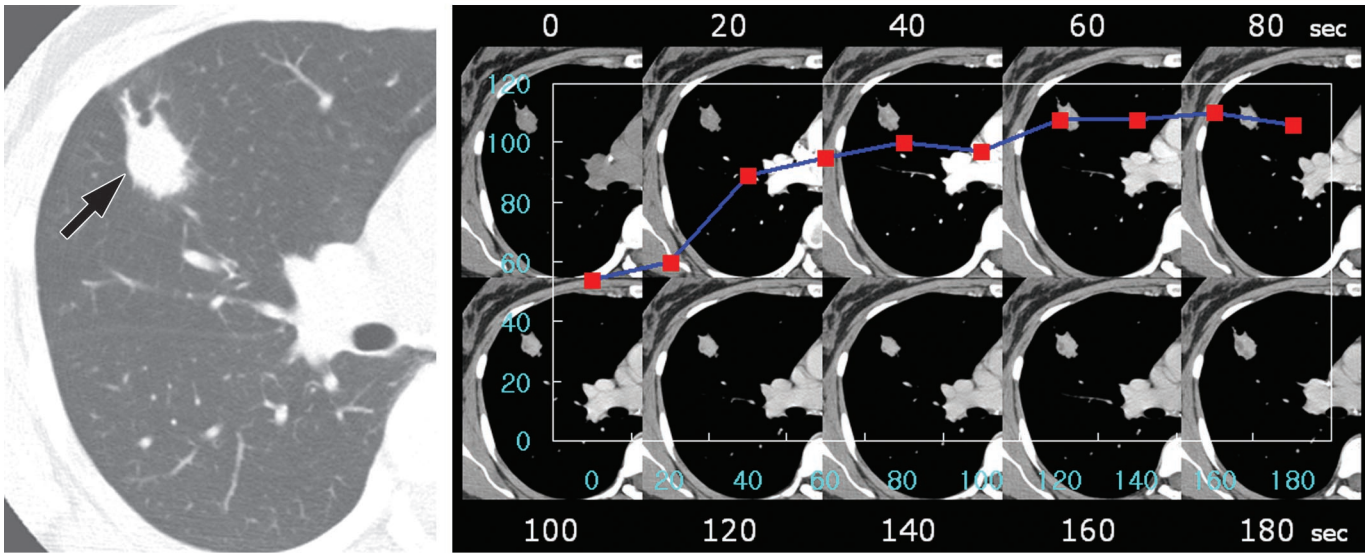

a. b.

Figure 4. Tuberculoma in a 45-year-old woman. **(a)** Lung window of transverse thin-section (2.5-mm collimation) CT scan obtained at level of bronchus intermedius shows 21-mm nodule (arrow) with lobulated and spiculated margin. **(b)** Serial images obtained at 20-second intervals and at similar levels show enhancement dynamics of nodule. Peak enhancement is 110 HU; net enhancement, 56 HU; maximum enhancement ratio, 1.040; slope of enhancement, 0.007; and time to peak enhancement, 160 seconds. Microvessel density with CD31 immunostaining was 85, and VEGF was 6 (not shown).

relatively large vessels (>0.1-mm inner diameter). Our results concur with this suggestion. Furthermore, a good correlation between peak enhancement and VEGF expression suggests that increased microvessel density results from increased VEGF expression. VEGF is a well-known powerful angiogenic factor, and VEGF and microvessel density have been reported to be prognostic factors of survival in patients with lung cancer (12,13,19). Peak enhancement is expected to be a good indicator of the extent of VEGF expression and to have a potential role as a prognostic factor, if it is acquired precisely by means of detailed dynamic enhancement with multi–detector row CT.

In the current study, the measured total organ dose at thin-section, dynamic, and low-dose CT ranged from 185.8 to 191.6 mGy at the sites of nodule location. Although this dose at the nodule location is about 10 times higher than that at single–detector row helical CT (18–19 mGy with 1–10-mm collimation, 120 kVp, and 300 mAs) (20) and four or five times higher than that with standard helical multi–detector row CT (38.7 to 39.5 mGy) at our institution, dynamic enhancement is not likely to be repeated in a patient who appears to have either a benign or a malignant nodule. If the result of dynamic enhancement CT suggests a benign enhancement pattern, then plain radiography or low-dose helical CT should be sufficient for follow-up imaging. When enhancement patterns appear to indicate malignancy, biopsy or surgery will be performed in most cases, and the rest will be followed up with plain radiography or conventional CT for suspicion of malignancy. Furthermore, use of low milliamperage at dynamic CT might have mitigated the radiation dose.

TABLE 6
Correlation between Extent of Nodule Enhancement and Tumor Angiogenesis

Parameter	Mean ± Standard Deviation	*R* Value*	*P* Value
Microvessel density	47.6 ± 25.2		
Peak enhancement (HU)	95.8 ± 20.0	0.369 (0.136)	.006
Net enhancement (HU)	52.6 ± 17.0	0.251 (0.063)	.067
VEGF	6.2 ± 2.5		
Peak enhancement (HU)	93.9 ± 22.8	0.277 (0.077)	.042
Net enhancement (HU)	50.3 ± 19.3	0.184 (0.034)	.182

* Pearson correlation coefficient. Numbers in parentheses are R^2 values.

A few limitations of this study were as follows. We obtained dynamic CT scans for only 3 minutes. With images acquired during 5 minutes or more, the washout dynamics of pulmonary nodule enhancement could have been obtained. In addition, we did not consider the morphology, as determined at thin-section CT of the nodule, for differentiation of benignancy and malignancy. We presume that well-defined round nodules at thin-section CT with homogenous enhancement of more than 30 HU at dynamic CT may suggest the possibility of a benign vascular tumor, such as a sclerosing hemangioma. A nodule with a spiculated margin seems worrisome enough to require biopsy or removal, regardless of findings of dynamic enhanced CT. In a tuberculosis-endemic area, however, up to 38% of benign nodules may show spiculated margin (21).

Our study may have selection bias. We excluded 57 patients who had neither histologic diagnosis nor follow-up information. However, most patients excluded were those who had no follow-up or had follow-up of less than 6 months. Some patients were excluded because they denied surgery or biopsy. In this study, we did not exclude any patients with regard

to specific surgery criteria or the results of our dynamic CT examination.

In conclusion, dynamic enhancement with multi–detector row CT shows a high sensitivity and a high negative predictive value for the diagnosis of malignant nodules, and the extent of enhancement at dynamic CT reflects the underlying extent of nodular angiogenesis.

References

1. Erasmus JJ, Connolly JE, McAdams HP, Roggli VL. Solitary pulmonary nodules. Part I. Morphologic evaluation for differentiation of benign and malignant lesions. RadioGraphics 2000; 20:43–58.
2. Swensen SJ, Morin RL, Schuleler BA, et al. Solitary pulmonary nodule: CT evaluation of enhancement with iodinated contrast material—a preliminary report. Radiology 1992; 182:343–347.
3. Swensen SJ, Brown LR, Colby TV, Weaver AL. Pulmonary nodules: CT evaluation of enhancement with iodinated contrast material. Radiology 1995; 194:393–398.
4. Yamashita K, Matsunobe S, Tsuda T, et al. Solitary pulmonary nodule: preliminary study of evaluation with incremental dynamic CT. Radiology 1995; 194:399–405.
5. Yamashita K, Matsunobe S, Takahashi R, et al. Small peripheral lung carcinoma evaluated with incremental dynamic CT: radiologic-pathologic correlation. Radiology 1995; 196:401–408.
6. Murayama S, Murakami J, Hashimoto S, Torii Y, Masuda K. Noncalcified pulmonary tuberculomas: CT enhancement patterns with histologic correlation. J Thorac Imaging 1995; 10:91–95.
7. Swensen SJ, Brown LR, Colby TV, Weaver AL, Midthun DE. Lung nodule enhancement at CT: prospective findings. Radiology 1996; 201:447–455.
8. Zhang M, Kono M. Solitary pulmonary nodules: evaluation of blood flow patterns with dynamic CT. Radiology 1997; 205:471–478.
9. Swensen SJ, Viggiano RW, Midthun DE, et al. Lung nodule enhancement at CT: multicenter study. Radiology 2000; 214: 73–80.
10. Hu H, He HD, Foley WD, Fox SH. Four multidetector-row helical CT: image quality and volume coverage speed. Radiology 2000; 215:55–62.
11. Weidner N, Semple JP, Welch WR, Folkman J. Tumor angiogenesis and metastasis-correlation in invasive breast carcinoma. N Engl J Med 1991; 324:1–8.
12. Fontanini G, Bigini D, Vignati S, et al. Microvessel count predicts metastatic disease and survival in non–small cell lung cancer. J Pathol 1995; 177:57–63.
13. Fontanini G, Vignati S, Boldrini L, et al. Vascular endothelial growth factor is associated with neovascularization and influences progression of non–small cell lung carcinoma. Clin Cancer Res 1997; 3:861–865.
14. Shibusa T, Shijubo N, Abe S. Tumor angiogenesis and vascular endothelial growth factor expression in stage I lung adenocarcinoma. Clin Cancer Res 1998; 4:1483–1487.
15. Miles KA. Tumour angiogenesis and its relation to contrast enhancement on computed tomography: a review. Eur J Radiol 1999; 30:198–205.
16. Ahn MJ, Jang SJ, Park YW, et al. Clinical prognostic values of vascular endothelial growth factor, microvessel density, and P53 expression in esophageal carcinomas. J Korean Med Sci 2002; 17:201–207.
17. Jung KJ, Lee KS, Kim SY, Kim TS, Pyeun YS, Lee JY. Low-dose, volumetric helical CT. Image quality, radiation dose, and usefulness for evaluation of bronchiectasis. Invest Radiol 2000; 35:557–563.
18. Ohno Y, Hatabu H, Takenaka D, Adachi S, Kono M, Sugimura K. Solitary pulmonary nodules: potential role of dynamic MR imaging in management-initial experience. Radiology 2002; 224:503–511.
19. Ohta Y, Endo Y, Tanaka M, et al. Significance of vascular endothelial growth factor messenger RNA expression in primary lung cancer. Clin Cancer Res 1996; 2:1411–1416.
20. McNitt-Gray MF. AAPM/RSNA physics tutorial for residents: topics in CT—radiation dose in CT. RadioGraphics 2002; 22:1541–1553.
21. Kim H, Kang SJ, Suh GY, et al. Predictors for benign solitary pulmonary nodule in tuberculosis-endemic area. Korean J Intern Med 2001; 16:236–241.